Biosensors and Bioelectronics 68 (2015) 336–342

Contents lists available at ScienceDirect

Biosensors and Bioelectronics

journal homepage: www.elsevier.com/locate/bios

Silicon nanonets for biological sensing applications with enhanced optical detection ability

P. Serre [a], V. Stambouli [b], M. Weidenhaupt [b], T. Baron [a], C. Ternon [a,b,*]

[a] Univ. Grenoble Alpes, CNRS, LTM, F-38000 Grenoble, France
[b] Univ. Grenoble Alpes, CNRS, LMGP, F-38000 Grenoble, France

ARTICLE INFO

Article history:
Received 22 October 2014
Received in revised form
27 December 2014
Accepted 2 January 2015
Available online 3 January 2015

Keywords:
Fluorescence sensor
DNA hybridization detection
DNA biochip
Nanonet
Silicon nanowire

ABSTRACT

Optical sensors based on fluorescence methods are used in numerous areas of society, ranging from healthcare to environmental monitoring. But the race to elaborate portable and highly sensitive detection systems leads to the huge development of nanomaterial-based sensors. Here, we have fabricated a silicon nanonet, or silicon nanowire (SiNW) network, -based biosensor for DNA hybridization detection by fluorescence microscopy. We demonstrate that by leveraging the properties of the SiNWs such as their large specific surface and the high aspect ratio, these nanonet sensors have significantly enhanced sensitivity and better selectivity compared to plane substrates. The fluorescence signal shows an intensity increasing with the SiNW density on the nanonet and for the denser nanonets, the detection limit for DNA hybridization is 1 nM. The elaborated Si nanonet-based DNA sensors present more than 50% change in fluorescence intensity between complementary DNA and 1 base mismatch DNA which shows their high selectivity. Finally, we have integrated the Si nanonet-based sensor into a DNA chip and we have shown that this selective sensor can be reproduced on a large scale area.

1. Introduction

It is believed that combining nanotechnologies and biotechnologies will result in a new class of multifunctional devices and systems for biological and chemical sensing characterized by better sensitivity and specificity and higher recognition rates compared with current solutions based on bulk materials (Fortina et al., 2005). Indeed, molecular biologists operate in the domain of molecular and cellular dimensions ranging from several nanometers (DNA molecules, viruses) to several micrometers (cells) while engineers work on reducing material dimensions reaching feature sizes as small as several nanometers. Nano-objects with important analytical applications include nanoparticles, nanopores, nanotubes and nanowires. Among them, silicon nanowires (SiNWs) have attracted an increasing interest in the last decades. By considering their semiconducting properties, precise doping control during growth, high aspect ratio and superior specific area along with surface functionalities of the native oxide shell surrounding the SiNWs, they are indeed very interesting for integration into chemical and biological sensors (Chazalviel et al., 2011; Demami et al., 2012). Previously, individual SiNWs were reported as the sensing material for the detection of nucleic acids (Gao et al., 2011; Hahm and Lieber, 2004), proteins (Stern et al., 2007; Wang et al., 2005) and viruses (Ahn et al., 2010; Lin et al., 2009). However, despite the great potential of such nanowires, the above-mentioned unique SiNW-based sensors usually entail several limitations such as high-cost and time-consuming methods for the integration of the SiNW into functional devices. Indeed, this integration necessitates that an individual nanowire be positioned at a precise location on a substrate, which requires expensive, complex and numerous technological steps.

In the field of biosensing, there are two main classes of signal transduction for biochemical recognition: labeled signal transduction techniques measuring a particle or molecule attached to a receptor and label-free techniques directly measuring physical effects caused by specific biochemical binding events (Gervais et al., 2011). The optical detection using labels is the simplest and the most pervasive detection method used. Particularly, direct detection using fluorescence is simple and very sensitive. Constant improvements of technologies (labels, light sources, detectors, etc.) have contributed to the high sensitivity of fluorescence microscopy. One other possible way to increase further the fluorescence signal is to optimize the surface on which the probe is immobilized. First, it is possible to increase the number of available

* Corresponding author at: Laboratoire des Matériaux et du Génie Physique (LMGP)-Grenoble-INP, Minatec, 3 parvis Louis Néel, CS 50257, 38016 Grenoble Cedex 1, France.
E-mail addresses: pauline.serre@cea.fr (P. Serre), valerie.stambouli-sene@grenoble-inp.fr (V. Stambouli), marianne.weidenhaupt@grenoble-inp.fr (M. Weidenhaupt), thierry.baron@cea.fr (T. Baron), celine.ternon@grenoble-inp.fr (C. Ternon).

http://dx.doi.org/10.1016/j.bios.2015.01.012
0956-5663/

sites for the labeled molecules while reducing steric hindrances and improving target accessibility. Second, working on the optical paths of the signal can increase the amount of excitation or emission light (Gervais et al., 2011).

Herein, we develop a material composed of randomly oriented SiNWs, that addresses these two issues. Also called “nanonets”, for NANOstructured NETworks (Gruner, 2007), such materials show several interesting properties arising either from their individual components, the NWs or nanotubes, or from the structural properties of the network itself (Ternon et al., 2013). First, due to the NWs, the surface area increases in comparison with thin films. As a consequence, it provides a higher probe immobilization capacity (Peterson et al., 2001) while reducing steric hindrance (Murthy et al., 2008). Second, due to the overall geometry, the fluorophore labeled targets are located at varying distances from the reflecting substrate, instead of a unique distance in case of flat surfaces. As a consequence, the optical path is more complex so that the reduction in fluorophore efficiency due to interference phenomena between excitation and emission light disappears (Murthy et al., 2008).

The nanonet elaboration can be carried out by various techniques such as direct growth (Kocabas et al., 2007) or self-assembly from solution for e.g. spray coating (Madaria et al., 2011; Scardaci et al., 2011), Langmuir–Blodgett (Acharya et al., 2006) or vacuum filtration (Mulazimoglu et al., 2013; Wu et al., 2004). The vacuum filtration method, used in this work, is particularly attractive since it enables low cost fabrication of nanonets that are homogeneous over large surfaces and present a wide range of thicknesses. Submonolayer coverage to over 1 μm thick with a precise control of the NW density in the nanonets (Serre et al., 2014, 2015) can be achieved.

In this paper, we describe the elaboration technique of silicon nanonets using the vacuum filtration method and we detail the integration of the silicon nanonet into DNA sensors by presenting the functionalization steps of the SiNW native oxide. We demonstrate the nanonet advantages for DNA hybridization detection by fluorescence, as well as their overall performances. For this purpose four parameters are studied: (i) the detection limit which is the smallest detectable target concentration, (ii) the sensitivity which shows a link between the signal variation of the sensor and the target concentration, (iii) the selectivity which describes the sensor's capacity to detect a target in presence of other species and (iv) the recyclability which expresses the possibility to reuse the sensor without deteriorating its properties. And finally, these sensors were integrated into a DNA chip on a large scale area.

2. Material and methods

2.1. Chemical reagents

APTES, (3-Aminopropyl)-triethoxysilane was bought from Carl Roth and glutaraldehyde 10% was bought from Sigma-Aldrich. Single-stranded DNA (ssDNA) was synthesized by Biomers or Apibio and the different DNA sequences used in this work are given in Table 1. The sensor was designed for the detection of ssDNA target hybridization with complementary ssDNA probes grafted on the sensor. The target was labeled with a cyanine (Cy3) fluorophore, and DNA hybridization was detected by fluorescence measurements. The DNA probes were diluted at 10 μM in a sodium phosphate solution (0.3 M, pH 9) and the target DNA sequences were diluted at concentrations between 0.2 nM and 30 μM in a hybridization solution composed of phosphate buffered saline 0.1 M and NaCl 0.5 M, in deionized water (pH 7).

2.2. Si nanonet fabrication

SiNWs were synthesized by reduced pressure chemical vapor deposition using the classical Vapor–Liquid–Solid mechanism (see Supplementary material). The obtained vertically standing SiNWs were then self-assembled by the vacuum filtration method forming the silicon nanonet (Wu et al., 2004). First, the SiNW solution was prepared by dispersing the SiNWs in 40 mL of deionized water using ultrasonic agitation for 5 min and this SiNW solution was characterized by absorption spectroscopy in order to qualitatively determine the SiNW amount in solution which is related to the SiNW density in the nanonet (Serre et al., 2013). The absorbance at 400 nm of the SiNW solution was fixed at 0.06. Then, the SiNW solution was filtered through a 0.1 μm porous nitrocellulose membrane (47 mm in diameter). As the solvent went through the pores, the nanowires were trapped on the membrane surface forming subsequently the Si nanonet with nanowires randomly oriented as shown on the SEM images of Figs. 3a and 4a. As described in Serre et al. (2015), a systematic SEM image analysis has been performed to determine surface coverage and NW density. Different volumes (20–160 mL) of the SiNW solution were filtered in order to prepare SiNW networks of controllable density, ranging from 10 to 120×10^6 NWs cm^{-2}.

2.3. Sensor design and use

The sensors designed in this work are based on a covalent ssDNA probe immobilization on the Si nanonet surface. First, the Si nanonets were transferred onto Si substrate by membrane dissolution in an acetone liquid bath for 30 min. Then, the DNA immobilization was conducted through a multistep procedure which was described in details in our previous study (Serre et al., 2013): (i) the hydroxylation of Si nanonets on Si substrate using oxygen plasma for 4 min; (ii) the functionalization of the SiNW surface and the Si substrate with an aminosilane (APTES) in vapor phase at 80 °C for 60 min followed by an annealing treatment at 110 °C during 60 min; (iii) the grafting of a cross-linker (glutaraldehyde, 10%) onto the APTES-functionalized surface for 90 min at room temperature and (iv) the immobilization of 10 μM ssDNA probes on the Si nanonet through covalent bonds and the $NaBH_4$, 0.09 M, treatment for 60 min in order to reduce imine bonds. After this

Table 1
ssDNA sequences used for the biochip fabrication (purchased from Apibio) and for the general study (purchased from Biomers).

	Function	Label	Sequence						
Biochip	*non-complementary Probe*	*nonCt-pDNA*	*5′-NH2-TTTTT*	*CCA*	*AGA*	*AAG*	*GAC*	*CCG*	*−3′*
	2 base mismatch Probe	*2bm-pDNA*	*5′-NH2-TTTTT*	*GAT*	*AAA*	***GA***C	*ACT*	*CTA*	*−3′*
	1 base mismatch Probe	*1bm-pDNA*	*5′-NH2-TTTTT*	*GAT*	*AAA*	***G***CC	*ACT*	*CTA*	*−3′*
	ssDNA Probe	**pDNA**	**5′-NH2-TTTTT**	**GAT**	**AAA**	**CCC**	**ACT**	**CTA**	**−3′**
	ssDNA Target	**Ct-tDNA**	**3′-AC**	**CTA**	**TTT**	**GGG**	**TGA**	**GAT**	**AC-Cy3-5′**
General study	*1 base mismatch Target*	*1bm-tDNA*	*3′-AC*	*CTA*	*TTT*	*G**C**G*	*TGA*	*GAT*	*AC-**Cy3**-5′*
	2 base mismatch Target	*2bm-tDNA*	*3′-AC*	*CTA*	*TTT*	*G**CA***	*TGA*	*GAT*	*AC-**Cy3**-5′*
	non-complementary Target	*nonCt-tDNA*	*3′-AC*	*TGG*	*CGC*	*AAT*	*CAC*	*TCT*	*AC-**Cy3**-5′*

last process, which allows stabilizing the covalent binding through amine bonds, the Si nanonets are functionalized with ssDNA probes and the sensors based on these nanonets are ready for use.

For sensor use and DNA hybridization detection, the DNA-modified nanonet is incubated at 42 °C for 45 min by immersion in the hybridization solution with one of the different ssDNA target sequences at various concentrations. To characterize the selectivity of the hybridization, four target-DNA sequences (Table 1), were used: the complementary ssDNA target (tDNA), two sequences with 1 or 2 base mismatches with respect to the pDNA (1bm-tDNA and 2bm-tDNA) and finally a non-complementary ssDNA sequence (nonCt-tDNA). Fluorescence measurements were carried out in order to detect whether hybridization occurred. The recycling of the sensor was obtained thanks to DNA denaturation carried out by immersing the hybridized Si nanonets in a NaOH 0.1 M solution during 60 min.

2.4. Characterization techniques

Scanning electron microscopy (SEM) images of the synthesized nanonets were obtained using a Zeiss ultra plus model from Gemini technology. Fluorescence measurements were performed in different modes after each hybridization and denaturation procedure in order to evaluate the hybridization rate. First an Olympus BX41M epifluorescence microscope coupled with a 100 W mercury lamp was used. Cy3 dyes were excited at 550 nm and emitted fluorescence recorded at 570 nm. Second, fluorescence measurements were performed with a confocal laser scanning microscope Zeiss LSM700 equipped with a 63 × oil objective (numerical aperture 1.4). The emission wavelength of the argon laser diode was set at 555 nm and confocal images were collected (pinhole set at 1 Airy Unit) using an MBS405 dichroic filter ranging from 560 to 700 nm. The Image Pro plus software was used for image analysis and to determine the fluorescence intensity inside the regions of interest. Therefore, for each fluorescence measurement in the epifluorescence mode, 6 images issued from 2 identical samples (3 images per sample) were acquired and analyzed: first the background signal, originating from a non-hybridized area of the sample, was deduced from the signal of interest. Second averaging over all images was done, so that the mean fluorescence intensity was obtained. For each mean fluorescence intensity, the minimum and the maximum of the measured intensities were used for the error bars.

2.5. DNA biochip

The DNA biochip was produced on commercial glass slides from Genewave Amplislide specially manufactured for fluorescence-based microarray applications. Such slides are coated with an optical thin film, which allows a 10 to 20-fold fluorescence signal enhancement (Choumane et al., 2005). The Si nanonet was transferred onto the 19 cm^2 glass slides and the DNA modification process was performed as described in Section 2.3. Then, four specific ssDNA probes (Table 1) were grafted on the chip using a robot (Microgrid II Compact from Biorobotics) according to the scheme given in Fig. 5a. Each robot pin spotted a few hundreds micrometers DNA droplet of 10 μM. Four pins were used and this process was repeated over most of the slide surface. For a given nanonet density, the spot diameter should be constant. Then, $NaBH_4$ stabilization treatments were applied as previously described. The DNA hybridization was performed at 42 °C for 60 min by immersion in the hybridization solution (Sigma H-7140) with the ssDNA target sequence at 1 μM. Then, post-hybridization rinsing was done and the slide was optically characterized using an Amplireader from Genewave.

3. Results and discussion

3.1. Nanonet advantages for DNA hybridization detection over flat surfaces

The DNA immobilization procedure described in Section 2.3 was first applied to Si nanonets with a NW density of 27×10^6 NWs cm^{-2} deposited on bare Si substrate and was also applied to bare Si substrate. The hybridization procedure was conducted with 1 μM of complementary target DNA. We have already shown that the fluorescence signal obtained from epifluorescence measurement on the nanonet exhibits a discrete distribution (Serre et al., 2013). To further investigate where the DNA hybridization is located, a confocal fluorescence microscope with better spatial resolution was used. On the fluorescence image

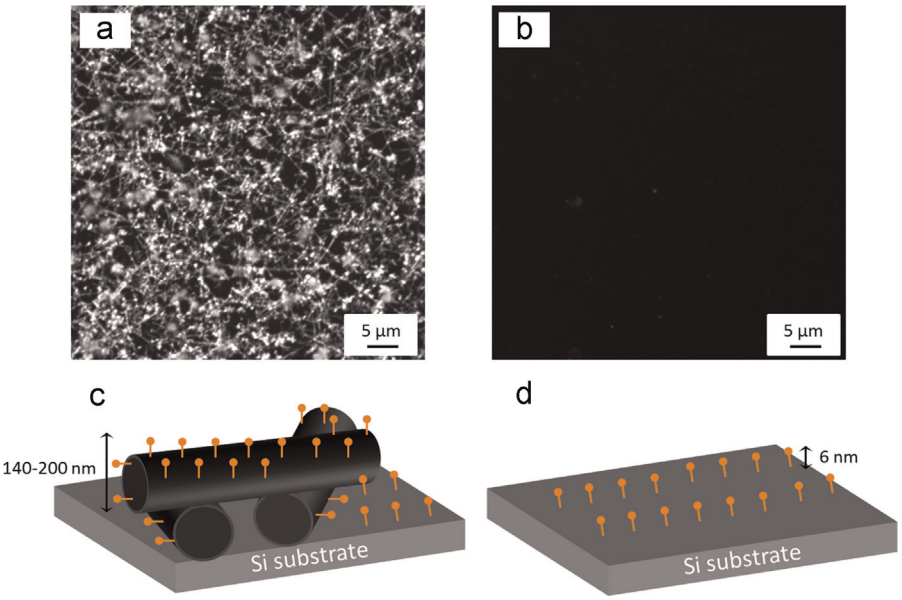

Fig. 1. Fluorescent images captured with a confocal laser scanning microscope (a,b) and schematic representation of the surface with double-stranded DNA localization (c,d) for silicon nanonets with a NW density of 27×10^6 NWs cm^{-2} (a,c) and bare Si substrate (b,d) after the DNA hybridization with a complementary Cy3-labeled DNA target.

(Fig. 1a), differences in the signal intensity coming from both the substrate and the Si nanonet can easily be seen. One can notice that the fluorescence emission is very high on the Si nanonet (mean value 1560 a.u.), whereas it is very low on the surrounding substrate (mean value 15 a.u.) as confirmed on the dark fluorescence image acquired on the bare substrate (Fig. 1b). Therefore, the fluorescence signal is enhanced by 2 orders of magnitude when a Si nanonet is added on silicon substrate. However, the larger surface area of the nanowires in comparison with a flat surface, which allows increasing the immobilized probe concentration and hence the number of available sites for target–probe recognition per surface unit does not explain such an increase. Indeed, the density of 27×10^6 NWs cm^{-2} leads to a small increase of surface area of 15.4%. Beside this geometrical effect, the Si nanonets provide an elevated layer for the fluorophore localization in comparison with plane substrates as illustrated in Fig. 1(c) and (d), which optimizes the interference from the reflecting Si surface (Murthy et al., 2008). As a consequence, in the case of the nanonet, the fluorescence signal is emitted over a large height (0–100 nm over the substrate on NWs and 0–200 nm in case of NW–NW junctions) while, in the case of bare silicon, the fluorescence signal is emitted at around 6 nm from the reflecting Si substrate. This last configuration implies destructive interferences, whereas the first configuration allows cumulative effects resulting in the 2 orders of magnitude enhancement (Bras et al., 2004).

To further evaluate the role of the surface area in hybridization detection enhancement, the effect of the SiNW density on the fluorescence response was investigated. As demonstrated in our previous work, the NW density of the nanonets is precisely controlled during the vacuum filtration process (Serre et al., 2014). As shown on Fig. 2a, for a fixed ssDNA target concentration (1 μM), the fluorescence intensity increases with NW density. Two regimes can be distinguished. For low densities ($< 30 \times 10^6$ NWs cm^{-2}), the observed quadratic increase suggests that the NW–NW junctions dominate the optical behavior. Indeed, on one hand, the junction number is proportional to the square of the NW density and on the other hand the cumulative effect previously described is enhanced on the junctions. For the highest densities (above 30×10^6 NWs cm^{-2}), the fluorescence signal seems to increase linearly with the NW density, suggesting that the silicon surface is too densely covered to allow reflection so that interference phenomena no longer occur. Fig. 2b displays the fluorescence intensity as a function of the target DNA concentration for various nanonet densities when exposed to complementary and non-complementary DNA target. With the help of an unfunctionalized nanonet characterized by fluorescence microscopy, it was possible to determine that a fluorescence signal lower than 3 a.u. corresponds to the noise and is not significant. To define the detection limit, we determined the concentration for which the specific signal is greater than the mean of the non-specific signal to which we add three times the standard deviation. In such a way, the false positive rate is 0.1%. In Fig. 2c, the detection limit is plotted as a function of the nanonet density.

As expected, the detection limit depends on the NW density. The lowest detection limit achieved in this study is 1 nM for Si nanonet-based sensors obtained with a density of 118×10^6 NWs cm^{-2}.

Thus, the nanonets used as DNA hybridization detectors exhibit two main advantages favoring a highly sensitive detection of biological species by fluorescence. The first one originates from cumulative effects of interference phenomena. The second one is geometrical and is based on the high surface area developed by the NWs. Therefore, we investigated the sensitivity, the selectivity and the reusability of the nanonet-based sensors with respect to the SiNW density.

3.2. Si nanonet-based DNA sensor characteristics

As shown above, the NW density in the nanonet plays a key role for the hybridization detection limit. A higher density allows

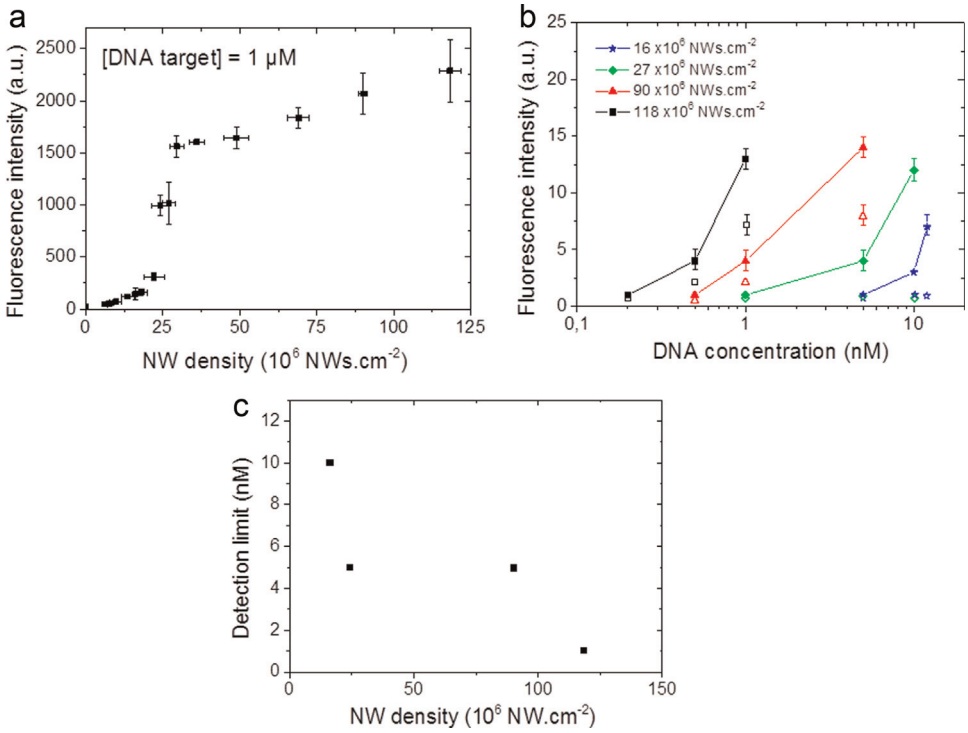

Fig. 2. (a) Fluorescence intensity as a function of SiNW density in the silicon nanonet with a DNA target concentration of 1 μM. (b) Fluorescence intensity as a function of the DNA concentration using nanonets with different nanowire densities when exposed to complementary (full symbol) and non-complementary (open symbol) DNA target. A fluorescence signal lower than 3 a.u. is not significant (noise). (c) Detection limit as a function of the SiNW density.

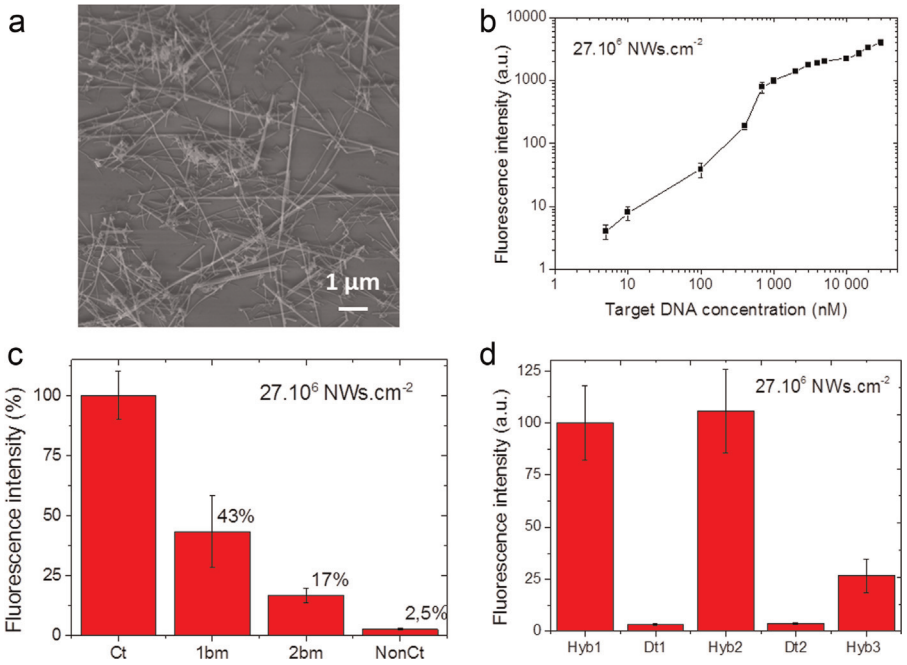

Fig. 3. Si nanonet-based DNA sensor characteristics for a NW density of 27×10^6 NWs cm^{-2}. (a) SEM image of the silicon nanonet. (b) Sensitivity as a function of the DNA target concentration. (c) Si nanonet-based DNA sensor selectivity. Normalized fluorescence intensity is shown for the complementary DNA sequence (Ct), the DNA with 1 (1bm) and 2 (2bm) base mismatches and the non-complementary DNA sequence (nonCt) for a ssDNA concentration of 1 μM. (d) Reusability of the DNA sensor.

to increase the fluorescence signal leading to a slight improvement of the detection limit (Fig. 2c), but it seems that higher NW densities are also detrimental for fluorescence sensitivity when the ssDNA target concentration is high as depicted on Fig. 2a (curve flattening at 30×10^6 NWs cm^{-2} for 1 μM ssDNA). Moreover, the substrate surface is totally covered by NWs when the density reaches 90×10^6 NWs cm^{-2}. Based on these experimental evidences, NW densities of 27×10^6 NWs cm^{-2} and 90×10^6 NWs cm^{-2} are investigated in the following.

3.2.1. *Low SiNW density nanonet-based biosensors*

First, DNA sensors based on low SiNW density nanonets (27×10^6 NWs cm^{-2}) were investigated. Results in terms of sensitivity, selectivity and reusability are plotted in Fig. 3. For the sensitivity study, the DNA target concentration was varied from 1 nM to 30 μM and the mean fluorescence intensities are plotted as a function of the ssDNA target concentration in Fig. 3b. As expected, the fluorescence signal increases with the ssDNA target concentration demonstrating the sensitivity of the Si nanonet-based DNA sensors. Moreover, the sensitivity is enhanced for low DNA concentrations (below 1 μM) for which a small variation in concentration leads to a more important variation in the intensity of the fluorescence signal in comparison to higher DNA concentrations.

The specificity of such sensors is also studied for a target DNA concentration in the hybridization solution of 1 μM. For this purpose, the nanonet-based sensor was incubated with different ssDNA sequences detailed in Table 1 (Ct-, 1bm-, 2bm- and nonCt-tDNA). The normalized fluorescence intensities recorded for each DNA sequence are reported in Fig. 3c. The highest signal (100%) is observed using complementary ssDNA and the lowest fluorescence response (2.5%) is obtained with non-complementary ssDNA. When the ssDNA sequence differs from the probe sequence with one or two bases an intermediate intensity is measured, 43% and 17% respectively. Such discrimination between the different target DNA sequences demonstrates that a low density nanonet-based sensor is selective enough allowing the monitoring of single base differences.

The last important characteristic of a biosensor is its potential for reuse which is defined as the number of DNA hybridization/DNA denaturation cycles that are possible without fluorescence signal loss after the hybridization process. The DNA denaturation is fully reversible when the physicochemical conditions are well chosen. In this work, the alcaline pH (NaOH, 0.1 M, 60 min) denaturation procedure was tested. Fig. 3d illustrates the successive hybridization/denaturation cycles by showing the fluorescence intensity variations after each step. One can notice that the denaturation is almost complete for the first cycle with the post-hybridization fluorescence fully recovering. However, after the second denaturation, the hybridization leads to a weaker fluorescence signal (26% of initial intensity). This phenomenon is attributed to silicon oxide etching by NaOH (Sakaino et al., 2000) and hence the loss of functionalized surface and the reduced ssDNA probe amount at the sensor surface. As a consequence, although well adapted for DNA denaturation, the alkaline process allows only one sensor recycling run. Further studies are conducted to optimize the denaturation process in relation to the sensor integrity.

3.2.2. *High SiNW density nanonet-based biosensors*

In this part, DNA sensors based on high SiNW density nanonets (90×10^6 NWs cm^{-2}) are investigated. As high NW densities are detrimental for fluorescence sensitivity when the ssDNA target concentration is high (Fig. 2a), only the results in terms of selectivity and reusability are plotted in Fig. 4. The target DNA concentration in the hybridization solution is 1 μM.

As depicted in Fig. 4b, it is noticeable that the selectivity of such sensors is very poor. Indeed, a high fluorescence signal is obtained with non-complementary ssDNA, reaching 55% of the fluorescence intensity obtained with the complementary ssDNA target. When the ssDNA sequences differ from the probe sequence with one or two bases an intermediate intensity is measured, with a value of 87% and 69%, respectively. The observed fluorescence may probably arise from non-specific adsorption of target DNA at the surface of the sensor based on high NW density nanonets. Indeed, due to the high specific area (increase of 50% in comparison with

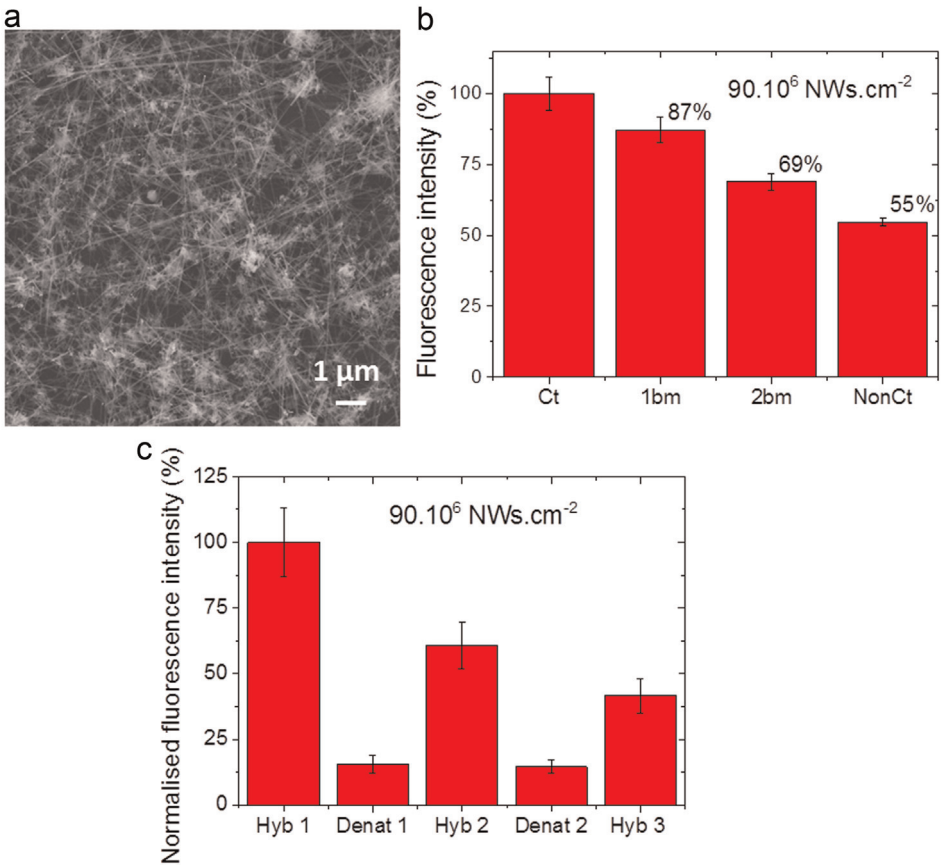

Fig. 4. Si nanonet-based DNA sensor characteristics for a NW density of 90×10^6 NWs cm^{-2}. (a) SEM image of the silicon nanonet. (b) Si nanonet-based DNA sensor selectivity. Normalized fluorescence intensity is shown for the complementary DNA sequence (Ct), the DNA with 1 (1bm) and 2 (2bm) base mismatches and the non-complementary DNA sequence (nonCt) for a ssDNA concentration of 1 μM. (c) Reusability of the DNA sensor.

flat surface), the opportunity for hydrogen bonds or any weak interaction forces between the functionalized surface and the tDNA increases drastically. As shown in Fig. 4a, when the NW density of the nanonets is as high as 90×10^6 NWs cm^{-2}, the surface is fully covered by the NWs while only 25% is covered in case of 27×10^6 NWs cm^{-2} (Fig. 3a). As a consequence, denser nanonets offer a high porosity due to the interlaced NWs that could trap the single DNA strands even after washing, leading to non-specific fluorescence signals.

For the DNA sensor recycling, the same phenomena as for low-density nanonets are observed as depicted in Fig. 4c. The alkaline denaturation leads to the progressive decrease of the ssDNA probes grafted on the nanonet by silicon oxide etching. One can notice that the ssDNA targets trapped between the NWs are partially removed through alkaline treatment.

3.2.3. Conclusion

Based on the previous results, it is noticeable that both NW density nanonets exhibit advantages for DNA hybridization detection but for different purposes. On one hand, DNA sensors with highest NW densities allow the detection of small amounts of DNA target, as low as 1 nM (Fig. 2b). But with high concentrations of DNA target, the non-specific adsorption is so high ($>$ 50%, Fig. 4b) that the sensor shows poor selectivity. On the other hand, the low NW-density nanonet-based DNA sensors are highly selective (Fig. 3c) and sensitive over a large range of DNA concentrations (from 5 nM to 30 μM, Fig. 3b) but the limit of detection only reaches the nanomolar range. As a consequence, depending on the purpose of the detection, it will be necessary to adapt the NW density in the nanonet and by combining several densities, it is possible to target all desired functionalities.

In the following part, we demonstrate that the Si nanonets can be easily integrated into standard DNA chips. For this purpose, nanonets with low density (27×10^6 NWs cm^{-2}) have been chosen.

3.3. Si nanonet-based DNA biochip

With the biochip, we want to make a proof of concept and to confirm that a single-stranded target DNA solution hybridizes differently on spots exposing different DNA probes immobilized on a nanonet. For the DNA biochip fabrication, a Si nanonet with a NW density of 27×10^6 NWs cm^{-2} was transferred onto a 19 cm^2 glass slide coated with a micrometer thin film dielectric mirror. Such elaborated biochips are composed of 14 patterns each of them being composed of 4 spots for each of the 4 ssDNA probe sequences (Table 1) as described on Fig. 5a, making in total 224 reaction zones on the chip surface. The fluorescence readout is given in image files showing the array of DNA hybridization spots. Part of this array (15%) is shown on Fig. 5b. Differences in fluorescence response are observed on this chip. First, the sensor selectivity is good with 1 base mismatch discrimination. Second, the fluorescence signal is reproducible from one spot to another for a given DNA probe sequence. Further studies are under investigation in order to develop a method for quantitative DNA determination using the biochip. Thus, the Si nanonet-based sensors elaborated in this work are successfully integrated into DNA chips with good performances in terms of selectivity and reproducibility on large scale areas.

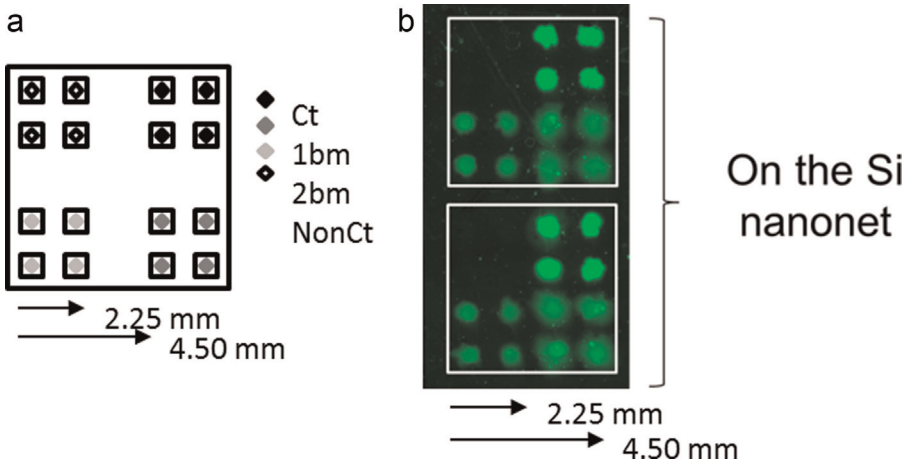

Fig. 5. (a) Scheme used for the grafting of the four specific ssDNA probes on the chip using a robot. (b) Fluorescence readout obtained with a DNA chip based on a Si nanonet with a NW density of 27×10^6 NWs cm^{-2} on a glass slide coated with a micrometer thin dielectric film using a DNA target concentration of 1 μM.

4. Conclusions

In summary, we have designed DNA sensors based on silicon nanonets that were integrated for the first time in DNA biochips. These nanowire networks have been elaborated by the vacuum filtration method, which is a low-cost fabrication technique compatible with large-scale applications. The nanonet geometry is attractive for DNA hybridization detection. Indeed, compared with DNA sensors with oligonucleotides directly grafted on plane substrates, the elaborated Si nanonet-based sensor with its large surface area and its ability to optimize interference phenomena increases the ssDNA probe availability and enhances DNA hybridization detection, respectively. Both of these properties improve the sensitivity of complementary DNA detection. This enhanced sensitivity has been demonstrated by a discrete fluorescence signal on Si nanonets, which is two orders of magnitude higher and by a decreased detection limit in comparison with plane substrates. Further, the influence of the SiNW density on the fluorescence signal and on the DNA sensor characteristics has also been demonstrated. The fabricated DNA sensors based on Si nanonets show a high sensitivity to DNA hybridization with a detection limit down to the nanomolar range. For Si nanonets with 27×10^6 NWs cm^{-2}, an excellent selectivity to complementary DNA targets has been evidenced with the capacity to discriminate 1 base mismatch in the DNA sequence. In order to increase the reusability of the sensor, the denaturation has to be optimized.

Finally, we integrate the Si nanonet-based sensors into DNA biochips at the macroscopic scale. In view of the improved performances of these chips compared with plane substrates, we believe that the Si nanonet-based DNA biochip could be integrated on lab-on-chip devices. Therefore, depending on the purpose, it is important to adapt the NW density in the nanonet.

For the future, two main points ensue from this study. First the nanonet is an interesting geometry for hybridization detection by fluorescence and further study should be conducted with other NW types in order to reduce the non-specific adsorption which is quite high with silica. Second, the Si nanonets are good candidates for DNA grafting and the next step consists in moving towards electrical detection of DNA hybridization (Serre et al., 2014).

Acknowledgements

The authors thank Pryanka Periwal and Thierry Luciani for the SiNW growth, Thomas Boudou for his help with the confocal microscope and Franz Bruckert and Catherine Picart for fruitful discussions on DNA sensors. This work was partly supported by the French RENATECH network. The research leading to these results has received funding from the European Community's Seventh Framework Programme (FP7/2007-2013) under grant agreement NANOFUNCTION no. 257375.

Appendix A. Supplementary material

Supplementary data associated with this article can be found in the online version at http://dx.doi.org/10.1016/j.bios.2015.01.012.

References

Acharya, S., Panda, A.B., Belman, N., Efrima, S., Golan, Y., 2006. Adv. Mater. 18, 210–213.
Ahn, J.-H., Choi, S.-J., Han, J.-W., Park, T.J., Lee, S.Y., Choi, Y.-K., 2010. Nano Lett. 10, 2934–2938.
Bras, M., Dugas, V., Bessueille, F., Cloarec, J.P., Martin, J.R., Cabrera, M., Chauvet, J.P., Souteyrand, E., Garrigues, M., 2004. Biosens. Bioelectron. 20, 797–806.
Chazalviel, J.-N., Allongue, P., Gouget-Laemmel, a. C., de Villeneuve, C.H., Moraillon, A., Ozanam, F., 2011. Sci. Adv. Mater. 3, 332–353.
Choumane, H., Ha, N., Nelep, C., Chardon, a., Reymond, G.O., Goutel, C., Cerovic, G., Vallet, F., Weisbuch, C., Benisty, H., 2005. Appl. Phys. Lett. 87, 031102.
Demami, F., Ni, L., Rogel, R., Salaun, A.C., Pichon, L., 2012. Sens. Actuators B: Chem. 170, 158–162.
Fortina, P., Kricka, L.J., Surrey, S., Grodzinski, P., 2005. Trends Biotechnol. 23, 168–173.
Gao, A., Lu, N., Dai, P., Li, T., Pei, H., Gao, X., Gong, Y., Wang, Y., Fan, C., 2011. Nano Lett. 11, 3974–3978.
Gervais, L., de Rooij, N., Delamarche, E., 2011. Adv. Mater. 23, H151–H176.
Gruner, G., 2007. Sci. Am. 17, 48–55.
Hahm, J., Lieber, C.M., 2004. Nano Lett. 4, 51–54.
Kocabas, C., Pimparkar, N., Yesilyurt, O., Kang, S.J., Alam, M.A., Rogers, J.A., 2007. Nano Lett. 7, 1195–1202.
Lin, C.-H., Hung, C.-H., Hsiao, C.-Y., Lin, H.-C., Ko, F.-H., Yang, Y.-S., 2009. Biosens. Bioelectron. 24, 3019–3024.
Madaria, A.R., Kumar, A., Zhou, C., 2011. Nanotechnology 22, 245201.
Mulazimoglu, E., Coskun, S., Gunoven, M., Butun, B., Ozbay, E., Turan, R., Unalan, H.E., 2013. Appl. Phys. Lett. 103, 083114.
Murthy, B.R., Ng, J.K.K., Selamat, E.S., Balasubramanian, N., Liu, W.T., 2008. Biosens. Bioelectron. 24, 723–728.
Peterson, a. W., Heaton, R.J., Georgiadis, R.M., 2001. Nucleic Acids Res. 29, 5163–5168.
Sakaino, K., Kawabata, Y., Adachi, S., 2000. J. Electrochem. Soc. 147, 1530–1534.
Scardaci, V., Coull, R., Lyons, P.E., Rickard, D., Coleman, J.N., 2011. Small 7, 2621–2628.
Serre, P., Ternon, C., Stambouli-Séné, V., Periwal, P., Baron, T., 2013. Sens. Actuators B: Chem. 182, 390–395.
Serre, P., Chapron, P., Durlin, Q., Francheteau, A., Lantreibecq, A., Ternon, C., 2014. 10th Conf. Ph.D Research Microelectronics and Electronics (PRIME) (June–July 2014), 1–4.
Serre, P., Mongillo, M., Periwal, P., Baron, T., Ternon, C., 2015. Nanotechnology 26, 015201.
Stern, E., Klemic, J.F., Routenberg, D.a., Wyrembak, P.N., Turner-Evans, D.B., Hamilton, A. D., LaVan, D.a., Fahmy, T.M., Reed, M.A., 2007. Nature 445, 519–522.
Ternon, C., Pauline, S., Rey, G., Holtzinger, C., Periwal, P., Martin, M., Baron, T., Stambouli, V., Langlet, M., 2013. Phys. Status Solidi RRL 7, 919–923.
Wang, W.U., Chen, C., Lin, K., Fang, Y., Lieber, C.M., 2005. Proc. Natl. Acad. Sci. USA 102, 3208–3212.
Wu, Z., Chen, Z., Du, X., Logan, J.M., Sippel, J., Nikolou, M., Kamaras, K., Reynolds, J.R., Tanner, D.B., Hebard, A.F., Rinzler, A.G., 2004. Science 305, 1273–1276.